Integrating Bimetallic MOF-Derived Sulfides with MnO_2: Synergistic Cu-Co-S@MnO_2 Heterojunctions for Flexible Hybrid Supercapacitors

Jiale Hou[1], Ziheng Huang[1], Haofeng Lu[1], Cheng Chen[1*], Xinfeng Wu[1], Yonghou Xiao[1], Wanghui Wei[2], Minjie Xue[2], Yanyun Ma[3], Xinzhou Ma[4], Shigang Sun[5], Donghai Lin[1]*

1.School of Energy and Materials, Shanghai Thermophysical Properties Big Data Professional Technical Service Platform, Shanghai Engineering Research Center of Advanced Thermal Functional Materials, Shanghai Key Laboratory of Engineering Materials Application and Evaluation, Shanghai Polytechnic University, Shanghai 201209, China.

2. Shanghai Institute of Measurement and Testing Technology, Shanghai 201203, China

3. Institute of Functional Nano & Soft Materials (FUNSOM), Jiangsu Key Laboratory for Carbon-Based Functional Materials & Devices, Soochow University, Suzhou, Jiangsu 215123, China

4. School of Materials Science and Hydrogen Energy, Foshan University, Foshan 528000, China

5. State Key Laboratory of Physical Chemistry of Solid Surfaces; Department of Chemistry, College of Chemistry and Chemical Engineering, Xiamen University, Xiamen, 361005, China

*Corresponding authors

E-mail: chencheng@sspu.edu.cn (Chen C.); dhlin@sspu.edu.cn (Lin D.)

Part I. Experimental section

Materials

Cobaltous Nitrate $6H_2O$ ($Co(NO_3)_2 \cdot 6H_2O$, Adamas, 99%), 1,2-Dimethylimidazole (MACKLIN, 98%), and Manganese(II) Nitrate Tetrahydrate ($Mn(NO_3)_2 \cdot 4H_2O$, Adamas, 99%), CTAB (cetyltrimethylammonium bromide, Adamas, 99%) were obtained from Adamas. Copper Nitrate Hydrate ($Cu(NO_3)_2 \cdot 5H_2O$, Adamas, 99%),

Sodium sulfide nonahydrate ($Na_2S·9H_2O$, Aladdin, 99%), potassium nitrate (KNO_3, Aladdin, 99%) were obtained from Aladdin.

Preparation of nickel foam

First, soak the nickel foam (NF) in acetone and ultrasonic treatment for a while (15-30 minutes) to remove the impurities such as oil on the surface, then take it out and rinse it with DI water. Put it into the dilute hydrochloric acid solution to soak properly (10-15 minutes), after soaking, rinse thoroughly with DI water to remove the residual hydrochloric acid. Next, the nickel foam is soaked in DI water and ultrasonicated for 15-30 minutes to further remove impurities and residues, then soaked in anhydrous ethanol and ultrasonicated for the same amount of time to remove water and other substances that may be left behind. The final overnight drying.

Preparation of Co-Cu-MOF@NF

Co-Cu-MOF@NF was synthesized by a simple hydrothermal method. First, 7.5 mmol of 2-methylimidazole was dissolved in a mixed solvent (30 mL of DI water and 5 mL of ethanol) and stirred to obtain solution A. Then, 2.4 mmol of $Co(NO_3)_2·6H_2O$ and 2.4 mmol of $Cu(NO_3)_2•5H_2O$ were dissolved in the same mixed solvent and stirred for 20 min to obtain solution B. Next, solutions A and B were quickly mixed, and the treated nickel foam substrate was immersed in the mixed solution and then placed in a stainless steel autoclave lined with polytetrafluoroethylene and hydrothermally reacted at 60 °C for 10 hours. After cooling, the products were washed repeatedly with DI water and ethanol and dried at 60 °C for 12 h to obtain Co-Cu-MOF@NF composites.

Preparation of Co-Cu-S@NF

A mixed solution containing 3 mmol Na_2S • $9H_2O$ and 40 mL DI water was transferred to a 50 mL PTFE-lined stainless steel autoclave along with the Co-Cu-MOF@NF sample, and the reaction was carried out at 140°C for 5 hours. At the end of the reaction, it was cooled naturally to room temperature, and the Co-Cu-S@NF sample was washed with DI water and ethanol and dried overnight.

Preparation of Co-Cu-S-MnO_2@NF

Co-Cu-S-MnO_2@NF was obtained by depositing MnO_2 on Co-Cu-S@NF using electrochemical deposition. A three-electrode system was used for the electrochemical deposition, in which the reference electrode was a saturated calomel electrode, the counter electrode was a platinum electrode, and the working electrode was Co-Cu-S@NF.

The electrodeposition solution was prepared by dissolving $Mn(NO_3)_2 \cdot 4H_2O$ solution with 0.24 M KNO_3 and 20 mg CTAB to obtain the electrodeposition solution.[1]

The electrodeposition was carried out using a CHI 660E electrochemical workstation with a constant voltage deposition method, the voltage was set at 1.2v and the deposition time was about 30 minutes.

Electrochemical measurements

To measure the electrochemical properties, the active materials Co-Cu-S-MnO_2@NF, Co-Cu-S@NF, and Co-Cu-MOF@NF (1 cm×1 cm) were used as working electrodes, the counter electrode was a platinum electrode, and a mercuric glycol electrode was used as a reference electrode, which was assembled into a three-electrode system in 3M KOH solution. The CV cycle test and Electrochemical Impedance Spectroscopy (EIS) were carried out at the CHI 660E electrochemical workstation, and the galvanostatic charge-discharge test (GCD) was carried out at the LAND electrochemical workstation.

Preparation of negative electrode material (AC/NF)

Slurry preparation: activated carbon (AC), acetylene black (conductive agent), and PVDF (binder) were mixed at a mass ratio of 8:1:1, and N-methylpyrrolidone (NMP) was added and ground to a homogeneous slurry.

Coating and drying: Coat the slurry uniformly on the surface of pre-treated NF ($1\times1cm^2$), vacuum dry at 60°C for 12 hours, and press the sheet under the pressure of 8-10 MPa to produce AC/NF negative electrode.

Preparation of solid gel electrolyte (PVA-KOH)

6 g PVA powder was added to 60 mL of DI water and stirred at 90°C until completely dissolved, while stirring, 3 M KOH solution was added and stirred for 30 min to form a transparent gel.

Assembly of asymmetric flexible supercapacitors

The positive electrode (Co-Cu-S-MnO_2@NF), electrolyte layer (PVA-KOH), and negative electrode (AC/NF) were stacked sequentially, covered with flexible PET film as an encapsulation layer, and sealed by pressing. The two-electrode system was tested by CV cycling on a CHI 660E electrochemical workstation and GCD on a LAND electrochemical workstation.

Part II. Calculations

Specific capacity calculation

The specific capacity was calculated by using the following equation:

$$C_f = \frac{I \times \Delta t}{m \times \Delta v}$$

Where I represents discharge current (A), Δt represents discharge time (s), m represents the mass of electroactive components (g) and Δv presents the potential window (V).

Determination and calculation of pseudocapacitor behavior

(1) Determination

The CV test obtained different peak current values (i., A) at different voltage scan rates (v, mV s^{-1}). Whether the electrode has diffusive or pseudocapacitive behavior during charging and discharging is discerned by corresponding the scan rate to the resulting peak current response.[2, 3]

$i = av^b$

$\log i = b\log v + \log a$

Obtain b-values (slopes) by linearly fitting $\log i$ and $\log v$

If the value of b is 0.5, the electrode material exhibits battery properties; if the value of b is in the range of 0.5-1, the electrode material exhibits both battery and pseudocapacitive properties; and if the value of $b \geqslant 1$, the electrode material exhibits pseudocapacitive properties.

(2) calculation

$$\frac{i}{v^{\frac{1}{2}}} = k_1 v^{\frac{1}{2}} + k_2$$

k_1 and k_2 are parameters that can be adjusted, and the value of k_1 can be obtained by a linear fit to $\frac{i}{v^{\frac{1}{2}}}$ and $v^{\frac{1}{2}}$ at the specified voltage.

Energy and power density

Energy and power density are calculated by the following equations:

$$E = \frac{C_f \Delta v^2}{2}$$

$$P = \frac{E}{\Delta t}$$

Where E (W h kg^{-1}) and P (KW kg^{-1}) are energy density and power density, respectively.

Software simulation

The CASTEP module in Materials Studio software was used, with the functional type being the Perdew - Burke - Ernzerhof (PBE) generalized gradient approximation (GGA). In the DFT calculations, the cutoff energy was 571.4 eV, and the Monkhorst - Pack scheme was used to sample the Brillouin zone, with a grid size of 3x3x1 for analyzing the density of states.

Part III. Supporting images

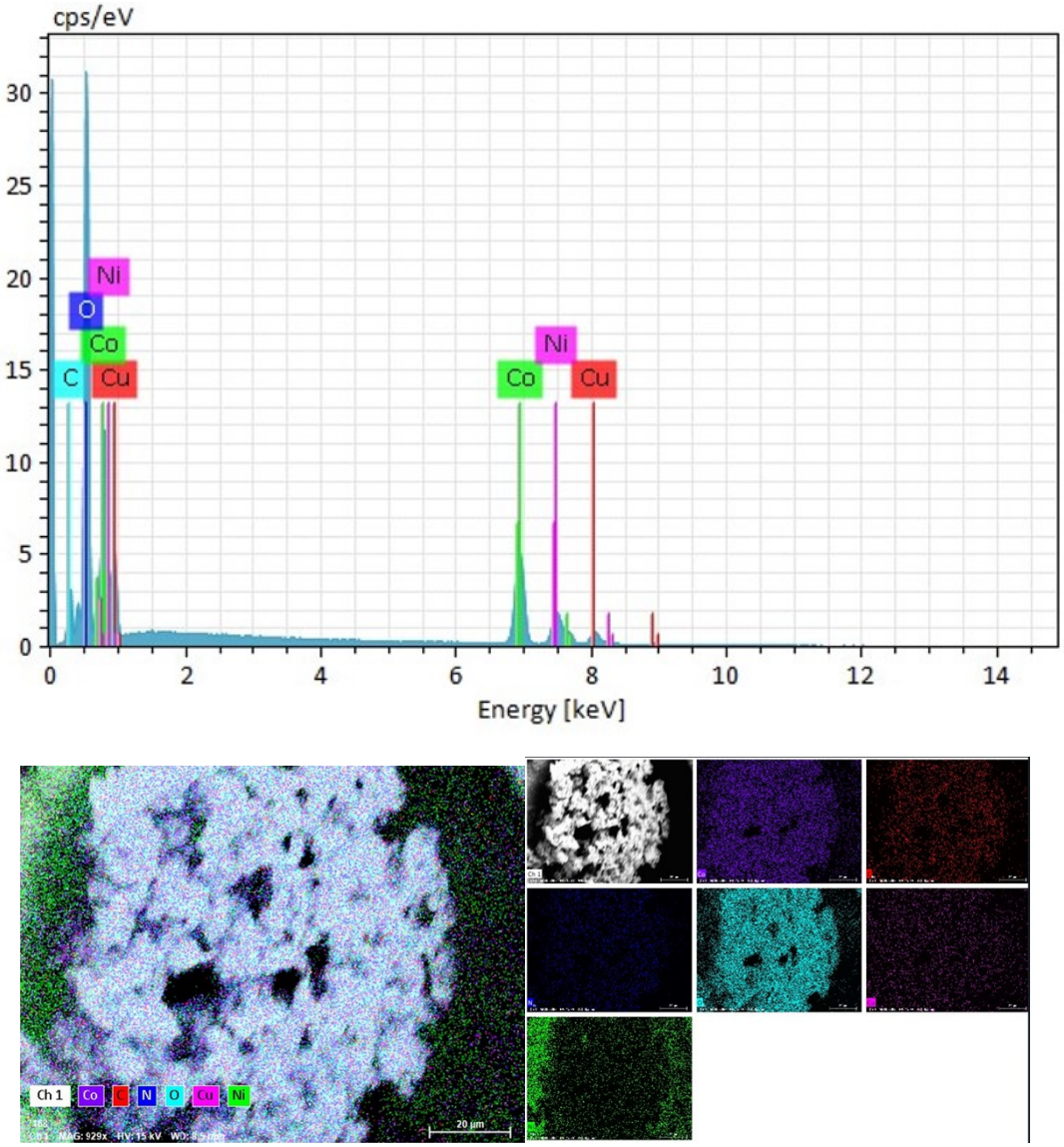

Figure S1 EDX spectra of Co-Cu-MOF/NF at low magnification.

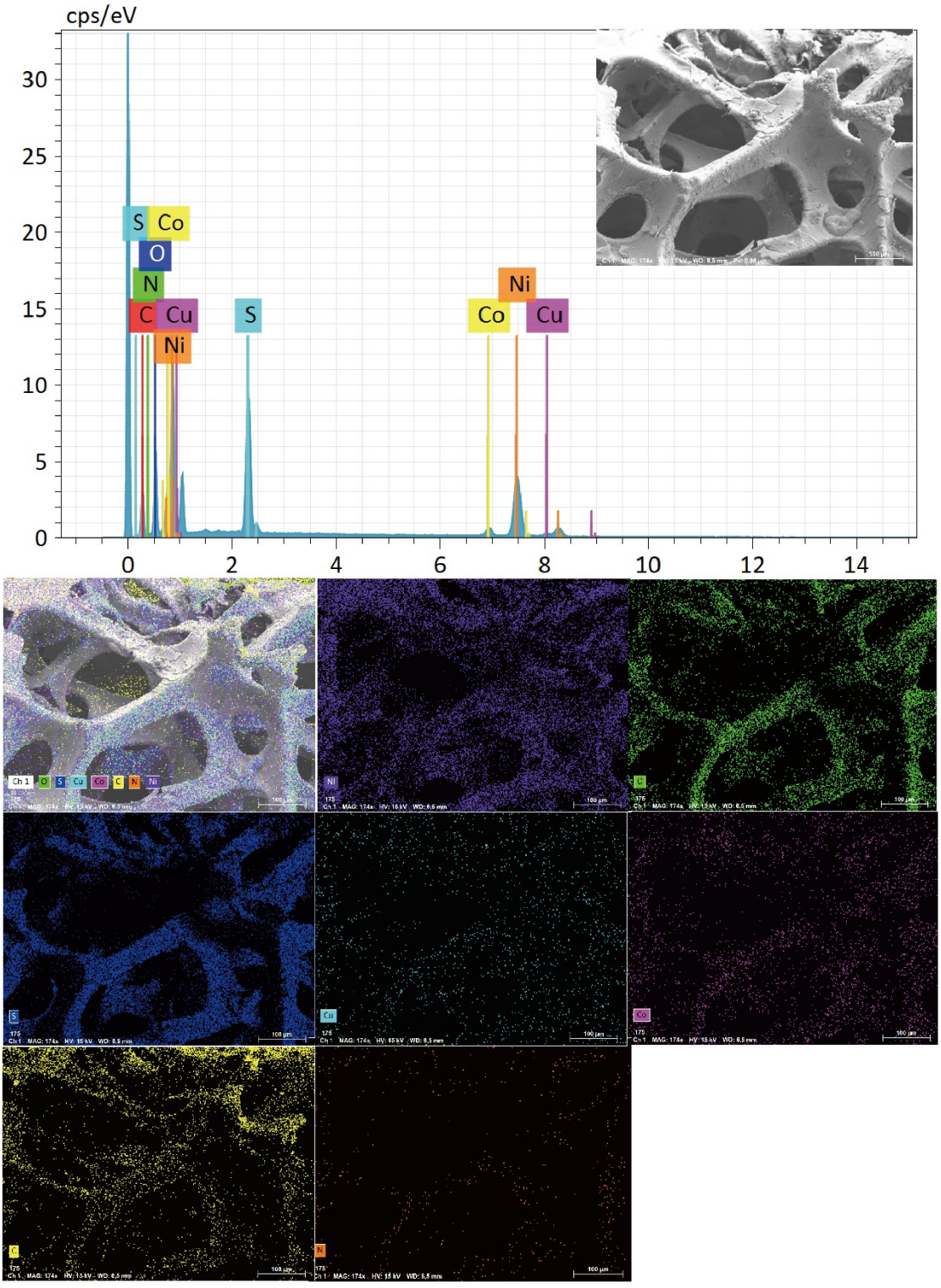

Figure S2 EDX spectra of Co-Cu-S/NF at low magnification.

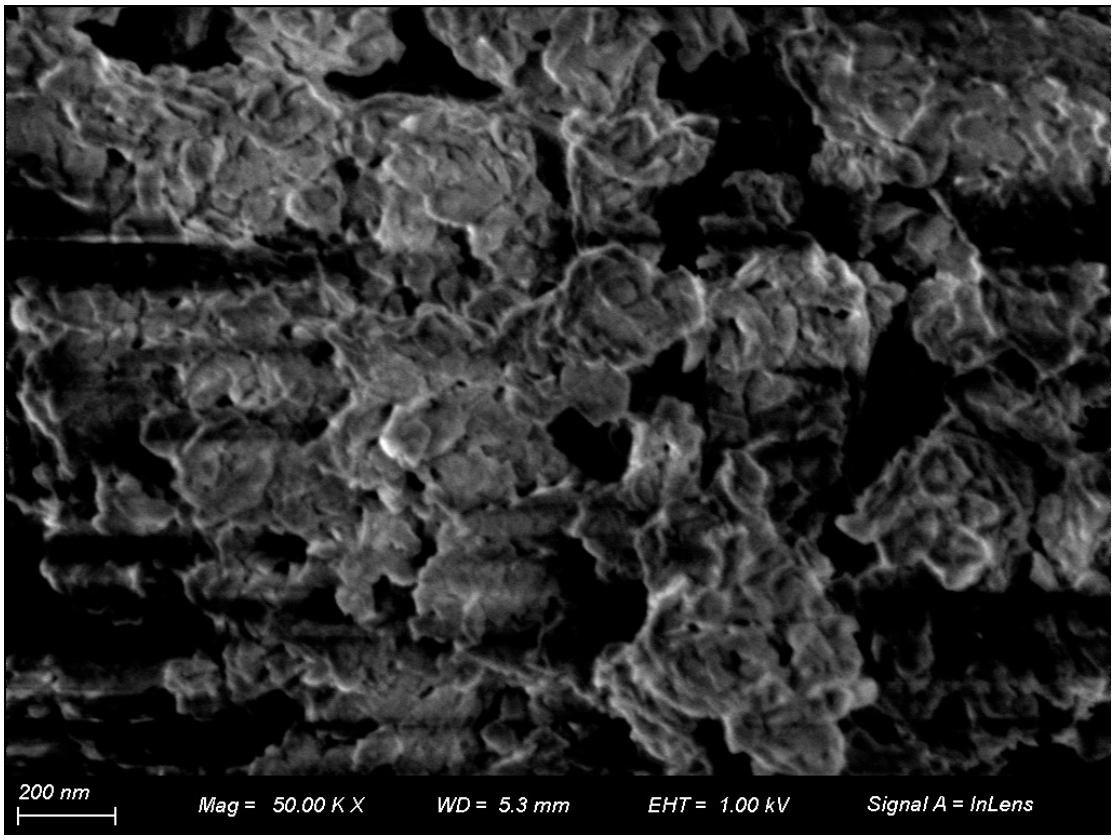

Figure S3 SEM image of Co-Cu-S-MnO_2@NF

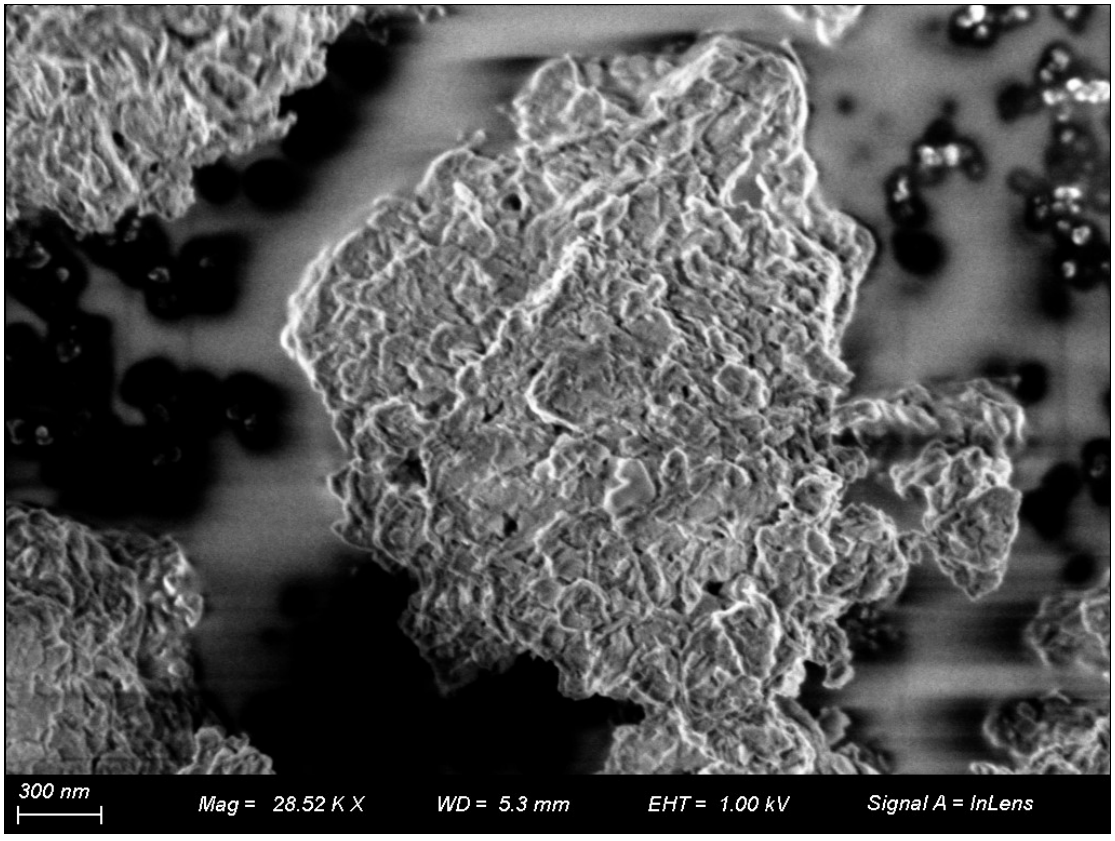

Figure S4 SEM image of MnO_2 thin film

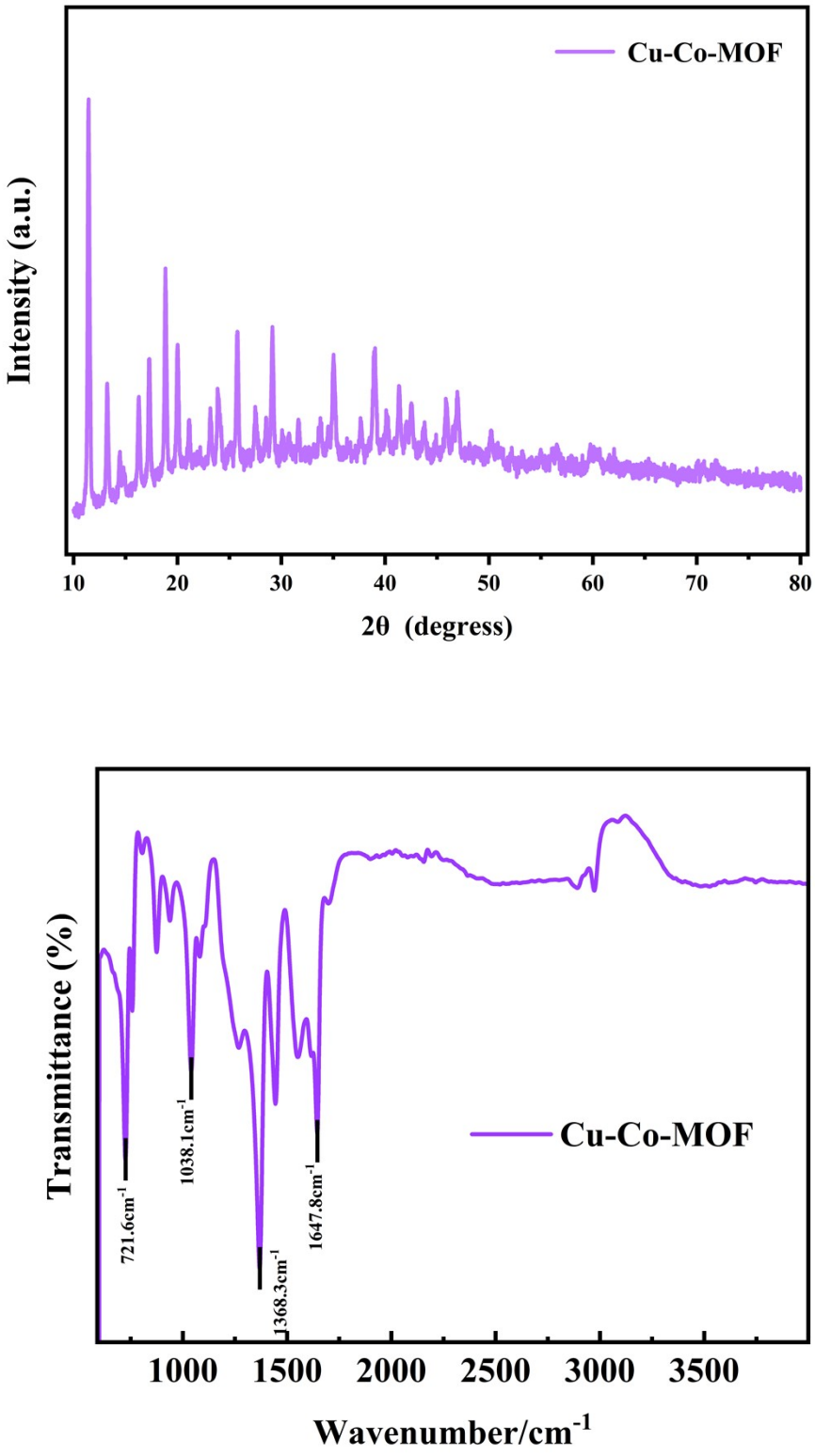

Figure S5 XRD mapping and FTIR of Co-Cu-MOF.

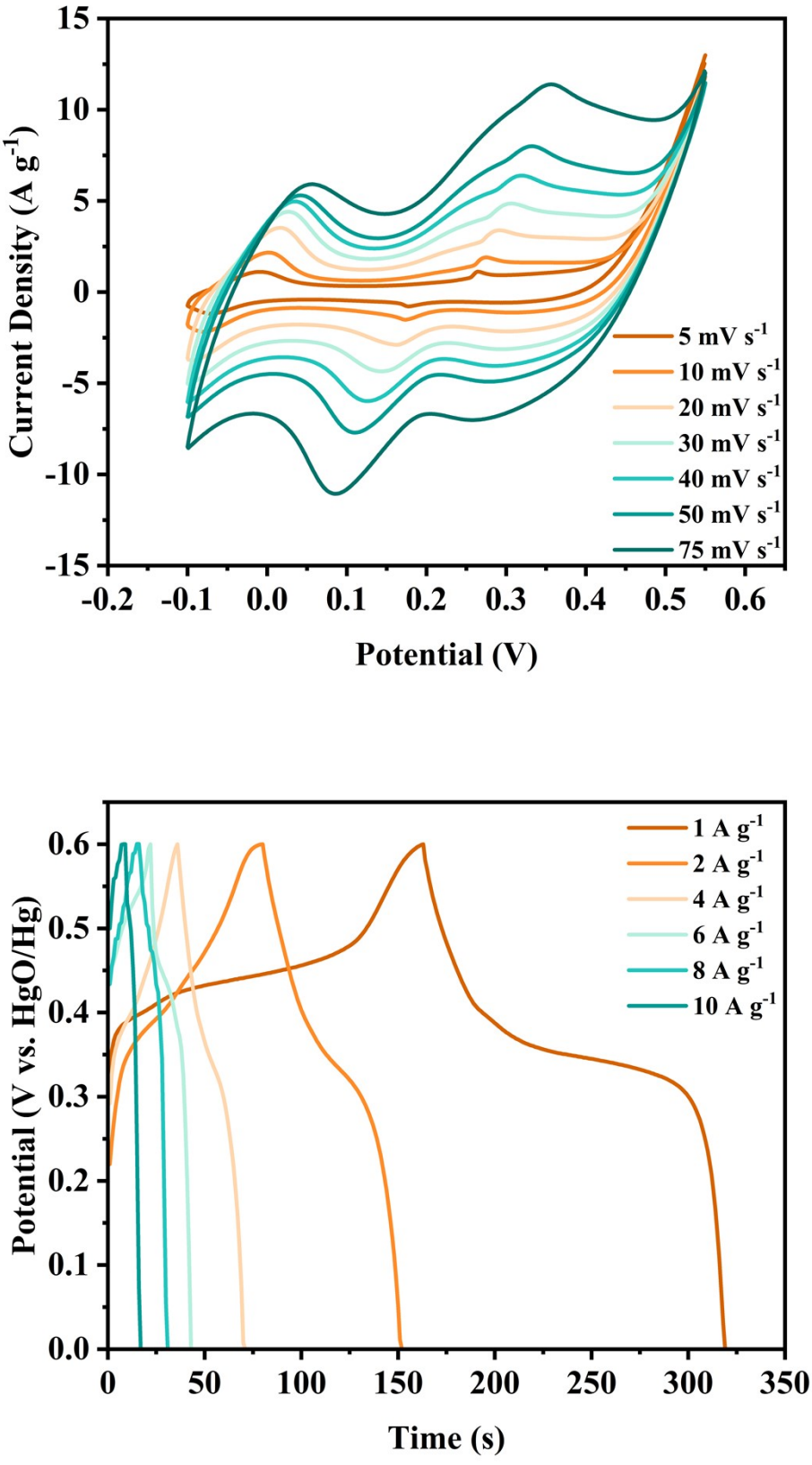

Figure S6 CV curves of Co-Cu-MOF@NF at different sweep speeds and GCD curves at different current densities.

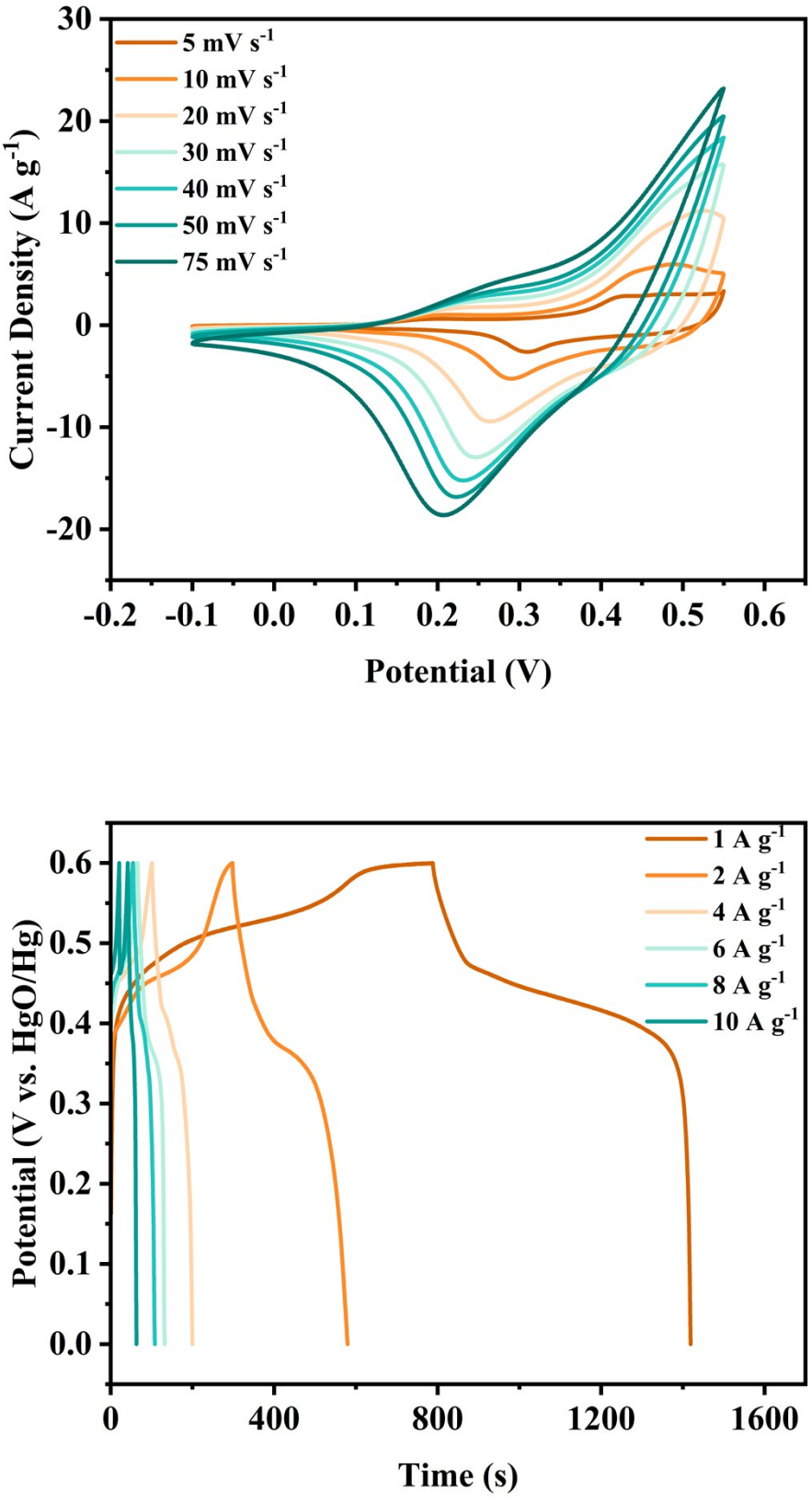

Figure S7 CV curves of Co-Cu-S@NF at different sweep speeds and GCD curves at different current densities.

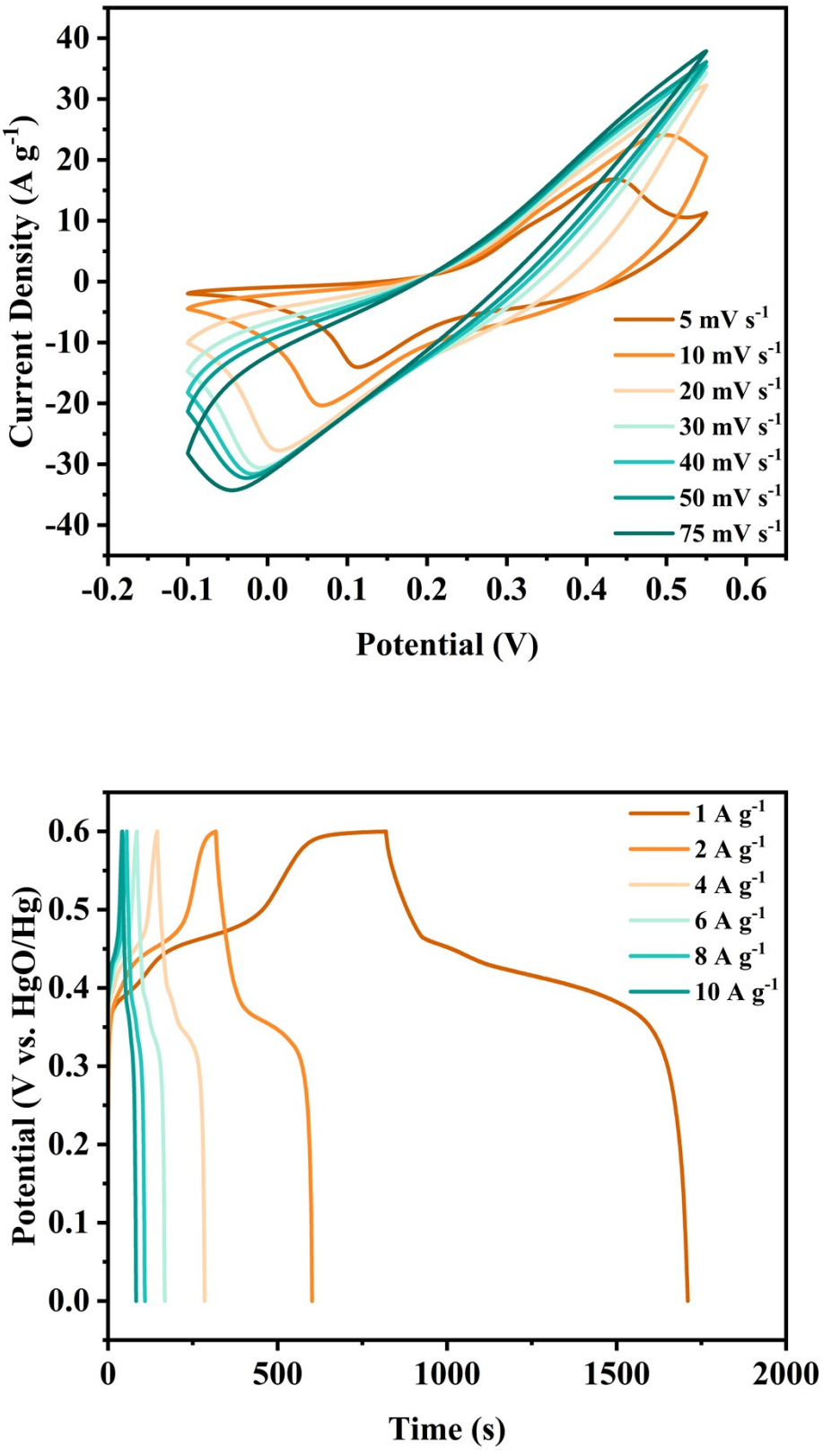

Figure S8 CV curves of Co-Cu-MnO_2@NF at different sweep speeds and GCD curves at different current densities.

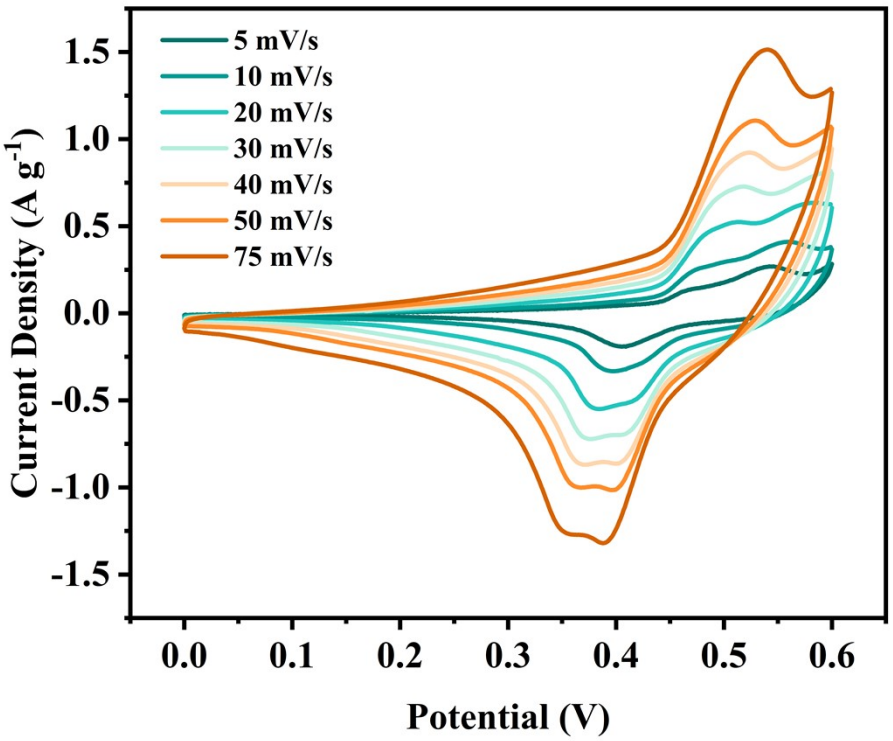

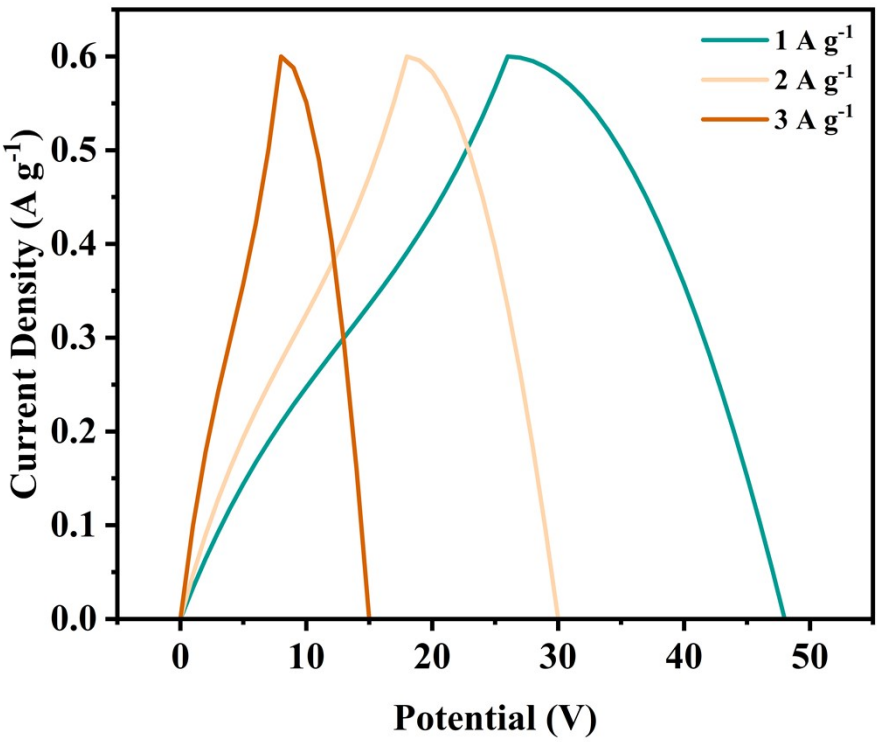

Figure S9 CV curves of NF at different sweep speeds and GCD curves at different current densities.

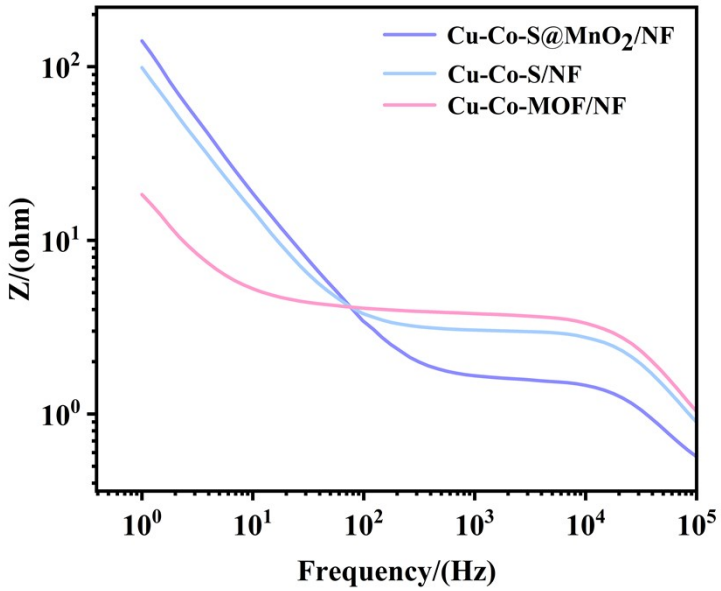

Figure S10 Bode plots of the three materials

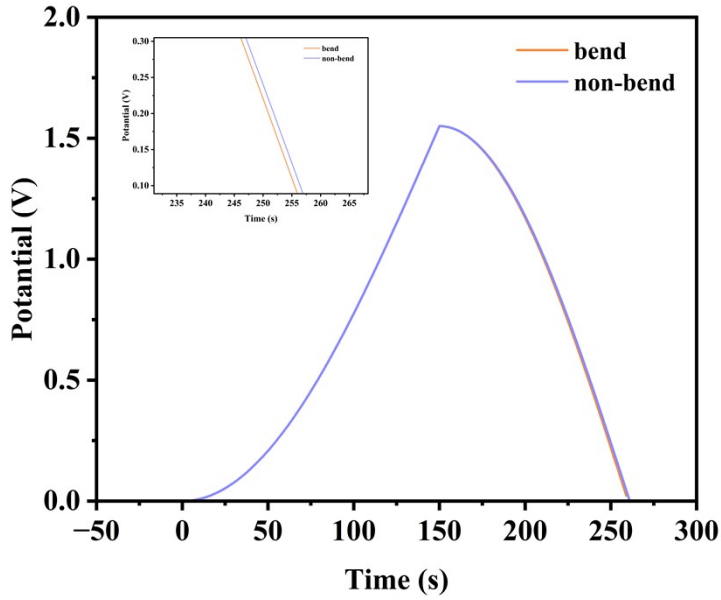

Figure S11 GCD profiles of the supercapacitor at various states.

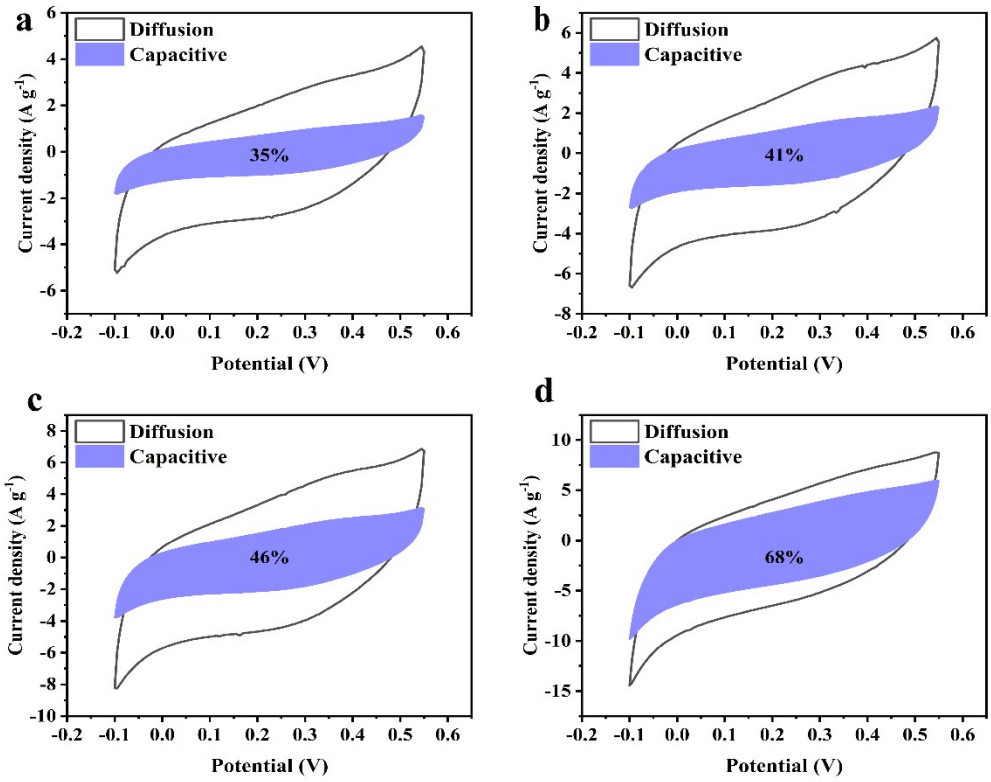

Figure S12 Pseudocapacitance contribution of Co-Cu-MnO_2@NF//AC at 20mV/s (a), 30mV/s (b),40mV/s (c),50mV/s (d) scan rate.

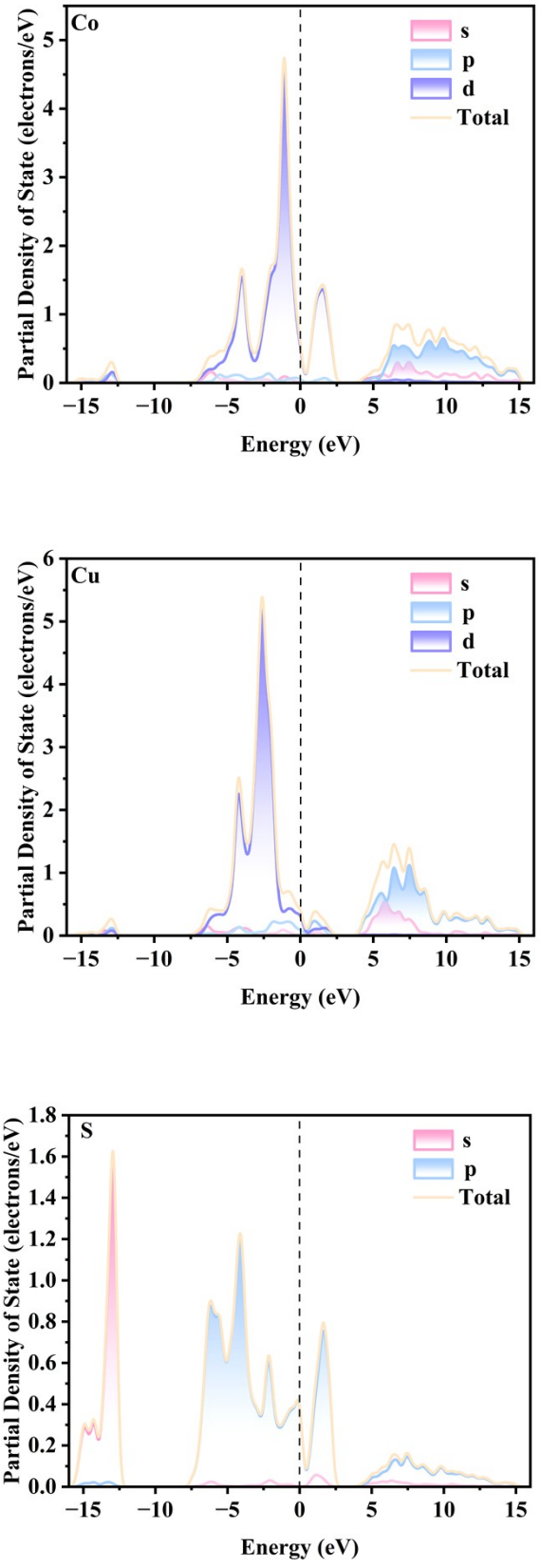

Figure S13 PDOS mapping of three elements in Cu-Co-S

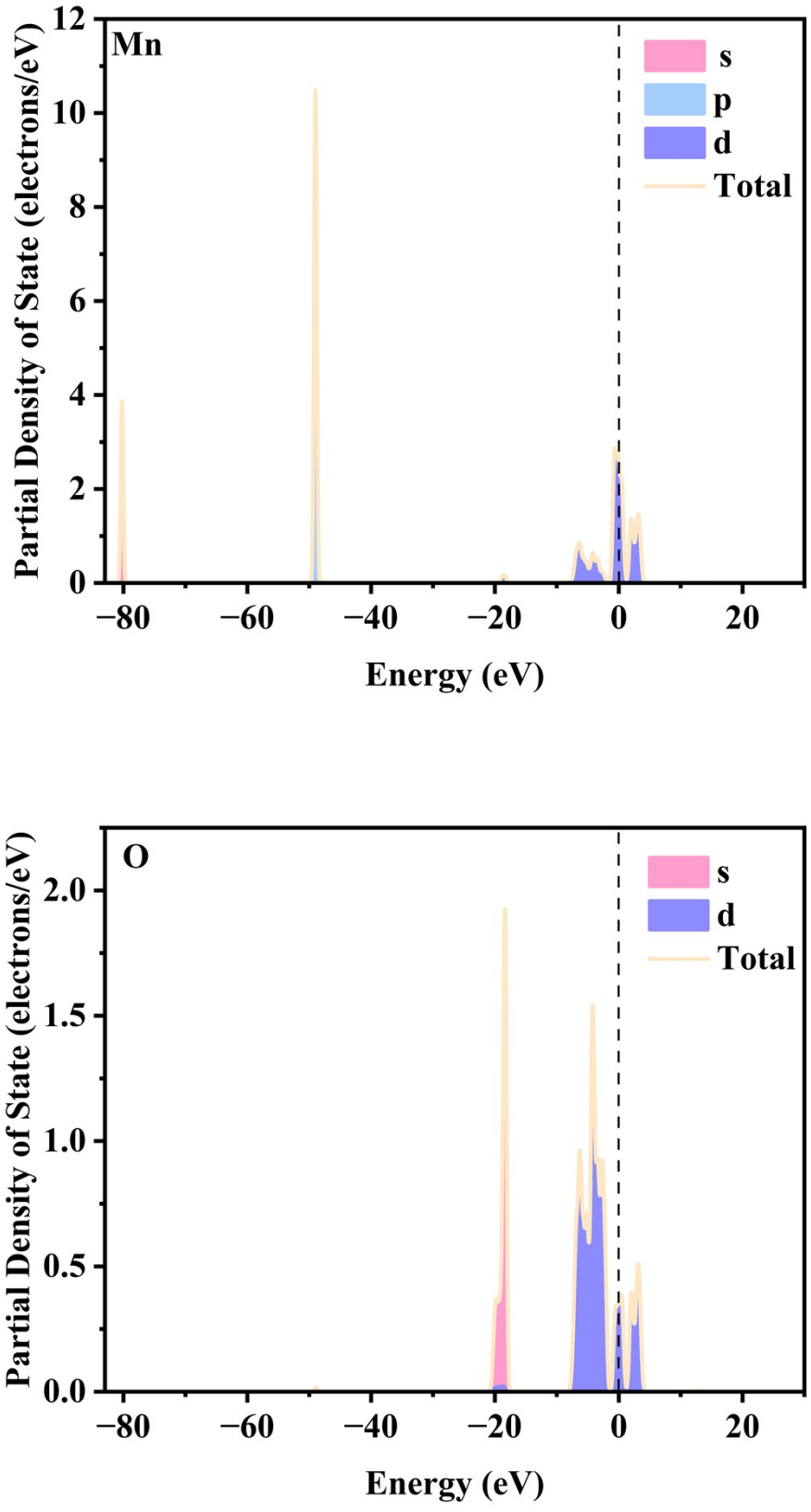

Figure S14 PDOS mapping of two elements in MnO_2

Part IV. Supporting table

Table S1 Elemental spectral data of Cu-Co-MOF/NF

Element	Atomic Number	Line	Normalized Mass/%	Atomic/%
O	8	K	34.91	56.84
Co	27	K	34.57	15.28
Ni	28	K	14.50	6.44
C	6	K	8.46	18.35
Cu	29	K	7.55	3.09
Total	—		100.00	100.00

Table S2 Elemental spectral data of Cu-Co-S/NF

Element	Atomic Number	Line	Normalized Mass/%	Atomic/%
Ni	28	K	48.08	22.11
C	6	K	19.34	43.47
S	16	K	13.34	11.23
O	8	K	11.75	19.83
Co	27	K	4.56	2.09
Cu	29	K	2.92	1.24
N	7	K	0.01	0.02
Total	—	—	100.00	100.00

Table S3 Elemental spectral data of Cu-Co-S@MnO_2/NF

Element	Atomic Number	Line	Normalized Mass/%	Atomic/%
O	8	K	42.20	53.27
Mn	25	K	23.67	8.70
Ni	28	K	12.24	4.21

C	6	K	10.82	18.19
N	7	K	10.67	15.38
S	16	K	0.41	0.26
Total	—	—	100.00	100.00

Table S4 Summary of capacity retention after cycling test found in the literature.

Electrode materials	**Electrolyte**	**Specific capacitance ($F\ g^{-1}$)**	**Current density ($A\ g^{-1}$)**	**Ref.**
$Cu_3(HHTATP)_2$	1 M KCl	339.5 ± 14.6 F g^{-1}	0.2 A g^{-1}	[4]
ZIF-67/PBA-derived sulfides	1M KOH	603.9 F g^{-1}	0.5A g^{-1}	[5]
CNF@CoNiS	3 M KOH	617.8F g^{-1}	0.5A g^{-1}	[6]
Cu/Co- MOF@G-NH_2	6 M KOH	874.3 F g^{-1}	1 A g^{-1}	[7]
Mn@Al-MOF	1M KOH	844 F g^{-1}	1 A g^{-1}	[8]
Ag@ZIF-8	3 M KOH	538.8 F g^{-1}	1 A g^{-1}	[9]
Zn-Co-MOF@CuO	3 M KOH	684 F g^{-1}	2 A g^{-1}	[10]
FL-MoS_2@rGO	1M KOH	346.1 F g^{-1}	1 A g^{-1}	[11]
Fe_2O_3@MnO_2	3 M KOH	449 F g^{-1}	1 A g^{-1}	[12]
ZnCo-MOF@PLB-800	3 M KOH	698.5F g^{-1}	1 A g^{-1}	[13]
CPO-CoNi	3 M KOH	580 F g^{-1}	1 A g^{-1}	[14]
Cu_3P/CoP	3 M KOH	804.3 F g^{-1}	1 A g^{-1}	[15]
FCNTs @Co-MOF	3 M KOH	590 F g^{-1}	1 A g^{-1}	[16]

MoS_2/Mn-MOF/MWCNT	3 M KOH	862.7 F g^{-1}	1 A g^{-1}	[17]
$Co_{6.53}$Ni-ZIF-L	3 M KOH	602 F g^{-1}	1 A g^{-1}	[18]
Al-MnO_2	1M Na_2SO_4	301.8 F g^{-1}	1 A g^{-1}	[19]
Cu-Co-S@MnO_2	3 M KOH	1483.3 F g^{-1}	1 A g^{-1}	This work

Table S5 Summary of energy and power densities found in the literature.

Electrode materials	Electrolyte	Energy density ($Wh\ kg^{-1}$)	Power density ($kW\ kg^{-1}$)	Ref.
Zn-In-S/C@CuO// Zn-In-S/C@CuO	3 M KOH	17	0.999	[20]
PTPAH@rGO2 PTPAH: N-containing conjugated microporous polymers	1 M H_2SO_4	11	3.345	[21]
Al-MnO_2//AC	PVA-Na_2SO_4 and PVA-KOH	64.7	1.3	[19]
3DCF//3DCF 3DCF: 3D Carbon Framework	$EMIMBF_4$	97	1	[22]
N-MXene/rGO//rGO	PVA-H_2SO_4	144.6	0.8759	[23]
MX/NCP//PNC MX/NCP: 2D MXene/Ni-Co phosphide PNC: porous nanocarbon	2 M KOH	54.3	0.5656	[24]
MSE-PC-500//MSE-PC-500 molten-salt-electrolysis porous carbon	6M KOH	9.7	0.3	[25]
Cu-Co-S@MnO_2//AC	PVA-KOH	185.25	0.75	This work

References

[1] Z. Wang, H. Wang, D. Pei, S. Wan, Z. Fan, M. Yu, H. Lu, Refinement of structural characteristics and supercapacitor performance of MnO2 nanosheets via CTAB-assisted electrodeposition, Progress in Natural Science: Materials International, 33 (2023) 881-890.

[2] F. Lu, Y. Ji, D. Shi, J. Yao, L. Pei, Electrochemically activated 3D Mn doped NiCo hydroxide electrode materials toward high-performance supercapacitors, Journal of Colloid and Interface Science, 641 (2023) 510-520.

[3] S. Fleischmann, J.B. Mitchell, R. Wang, C. Zhan, D.-e. Jiang, V. Presser, V. Augustyn, Pseudocapacitance: From Fundamental Understanding to High Power Energy Storage Materials, Chemical Reviews, 120 (2020) 6738-6782.

[4] G. Lee, G. Park, S.S. Park, Molecular-Level Pore Tuning in 2D Conductive Metal–Organic Frameworks for Advanced Supercapacitor Performance, Journal of the American Chemical Society, 146 (2024) 29767-29772.

[5] D. Yu, N. Li, H. Ding, Z. Shen, Y. Chen, T. Pan, X. Wu, X. Guo, H. Pang, Nano ZIF-67/PBA derived core-shell sulfides or phosphides for enhanced electrochemical performance of supercapacitors, Journal of Energy Storage, 95 (2024) 112608.

[6] G. Liu, F. Zhou, K. Yan, C. Zhuang, Y. Wang, C. Wang, D. Tian, In situ growth of Co3S4/Ni3S4 on electrospun ZIF-67 nanofibers for high-performance supercapacitor, Journal of Energy Storage, 94 (2024) 112462.

[7] J. Singh, A. Choudhury, M.W. Ahmad, A. Syed, H.A. Al-Shwaiman, M. Subramaniam, D.-J. Yang, 3D hierarchically structured copper/cobalt metal-organic frameworks grown on aminated graphene for solid-state asymmetric supercapacitors, Journal of Alloys and Compounds, 1014 (2025) 178638.

[8] M.R. Tamtam, R. Wang, R. Koutavarapu, G.S. Choi, J. Shim, Core-shell Mn@Al-MOF: A multidimensional hierarchical advanced electrode material for high-performance supercapacitors, Journal of Alloys and Compounds, 1013 (2025) 178517.

[9] M.R. Karim, C.-H. Choi, A. Mohammad, T. Yoon, Fabrication of high-performance supercapacitor of surface-engineered ZIF-8 for energy storage applications, Journal of Energy Storage, 93 (2024) 112199.

[10] I. Hussain, S. Iqbal, T. Hussain, W.L. Cheung, S.A. Khan, J. Zhou, M. Ahmad, S.A. Khan, C. Lamiel, M. Imran, A. AlFantazi, K. Zhang, Zn–Co-MOF on solution-free CuO nanowires for flexible hybrid energy storage devices, Materials Today Physics, 23 (2022) 100655.

[11] Y. Zhang, J. Xu, S. Lu, H. Li, T. Yonar, Q. Hua, T. Liu, Y. Zhang, Engineering few-layer MoS2 and rGO heterostructure composites for high-performance supercapacitors, Advanced Composites and Hybrid Materials, 8 (2025) 108.

[12] J. Li, S. Wu, X. Sun, J. Wang, J. Yang, X. Xu, Q. Hu, Y. Sun, Z. Wang, S. Kang, J. Liu, The rational design of Fe2O3@MnO2 derived from Fe[Fe(CN)6]·4H2O as

negative electrode for asymmetric supercapacitor, Journal of Energy Storage, 96 (2024) 112676.

[13] X. Ma, Y. Bai, S. Chen, Z. He, P. Wu, Y. Qi, S. Zhang, A composite of pineapple leaf-derived porous carbon integrated with ZnCo-MOF for high-performance supercapacitors, Physical Chemistry Chemical Physics, 26 (2024) 28746-28756.

[14] M. Yang, Q. Liu, M. Zhang, Y. Deng, C. Liu, F. Hu, X. Jian, Y. Chen, Preparation of CoNi-LDH-Modified Polypropylene-Based Carbon Fiber Membranes for Flexible Supercapacitors, Journal of Applied Polymer Science, n/a (2025) e56716.

[15] H. Zhou, R. Nasser, L. Zhang, Z. Li, F. Li, J.-M. Song, Copper/Cobalt based metal phosphide composites as positive material for supercapacitors, Chemical Engineering Journal, 496 (2024) 154102.

[16] O.A.A. El-Shamy, M.R. Siddiqui, G. Mele, Q. Mohsen, M.M. Alhajeri, M.A. Deyab, Synthesis, characterization and application of CNTs@Co-MOF and FCNTs@Co-MOF as superior supercapacitor: Experimental and theoretical studies, Journal of Molecular Structure, 1321 (2025) 140161.

[17] W. Peng, N. Song, Z. Su, J. Wang, K. Chen, S. Li, B. Wei, S. Luo, A. Xie, Two-dimensional MoS2/Mn-MOF/multi-walled carbon nanotubes composite material for high-performance supercapacitors, Microchemical Journal, 179 (2022) 107506.

[18] H. Ding, Z. Liu, J. Xie, Z. Shen, D. Yu, Y. Chen, Y. Lu, H. Zhou, G. Zhang, H. Pang, Ion Exchange‐Mediated 3D Cross‐Linked ZIF‐L Superstructure for Flexible Electrochemical Energy Storage, Angewandte Chemie International Edition, 63 (2024).

[19] J. Yan, C. Liu, J. Yang, Z. Wang, W. Yao, L. Huang, J. Cui, J. Liu, X. Hu, Y. Wu, A 2.6 V Flexible Supercapacitor Based on Al-MnO2-Na2SO4//AC-KOH with High Specific Energy, ACS Energy Letters, 8 (2023) 2033-2041.

[20] I. Hussain, M.Z. Ansari, C. Lamiel, T. Hussain, M.S. Javed, T. Kaewmaraya, M. Ahmad, N. Qin, K. Zhang, In Situ Grown Heterostructure Based on MOF-Derived Carbon Containing n-Type Zn–In–S and Dry-Oxidative p-Type CuO as Pseudocapacitive Electrode Materials, ACS Energy Letters, 8 (2023) 1887-1895.

[21] L. Teng, J. Duan, H. Liu, X. Zhang, J. Li, Y. Li, J. Hong, W. Lyu, Y. Liao, A conjugated microporous polymer–graphene composite porous sandwich-like film for highly efficient flexible supercapacitors, Journal of Materials Chemistry A, 12 (2024) 12423-12434.

[22] C. Leng, Z. Zhao, Y. Song, L. Sun, Z. Fan, Y. Yang, X. Liu, X. Wang, J. Qiu, 3D Carbon Frameworks for Ultrafast Charge/Discharge Rate Supercapacitors with High Energy-Power Density, Nano-Micro Letters, 13 (2020) 8.

[23] L. Liu, L. Huang, S. Yan, W. Shi, S. Li, X. Chen, J. Liu, Heteroatom doped S, N-MXene/rGO flexible film for supercapacitor applications, Chemical Engineering Journal, 506 (2025) 160320.

[24] E. Baasanjav, K.A.S. Raj, H. Hakkeem, C.S. Rout, S.M. Jeong, High-performance asymmetric supercapacitors based on 2D MXene/NiCoP hybrid and ZIF derived porous nanocarbon, Journal of Materials Science & Technology, (2025).

[25] Z. Qiao, N. Li, Y. Deng, D. Ji, D. Ji, D. Yuan, W. Song, Z. Li, H. Wu, Fabrication of nano-carbon cages via molten salt CO2 electrolysis for high-performance symmetrical supercapacitor, Nano Energy, 136 (2025) 110704.